JFM RAPIDS
journals.cambridge.org/rapids

Merging of a row of plumes or jets with an application to plume rise in a channel

G. G. Rooney†

Met Office, FitzRoy Road, Exeter EX1 3PB, UK

The physical interpretation of velocity potential is used to propose a model of
the mean flow boundary of a row of plumes or jets. Generalised plume equations
incorporating the plume area and net entrainment are closed with an entrainment
assumption. The resulting model is shown to approach the appropriate limiting
similarity solutions above and below the merging height in an unstratified environment.
The virtual origin of the far-field flow is hence predicted. An application to plume
rise in channels of varying aspect ratio shows that the model may be used to predict
the depth of the outflow along the channel.

Key words: convection in cavities, jets, plumes/thermals

1. Introduction

The merging of buoyant jets from proximate sources is a common occurrence in the
atmosphere and the ocean, likewise the motion of a plume in a restricted environment.
These flows have a common feature in that external influences interrupt the free rise
of buoyant fluid from a localised source. The merging problem has been the subject
of several studies, for pairs and rows of plumes as well as other configurations (Kaye
& Linden 2004; Cenedese & Linden 2014, and references therein). In particular, Lai
& Lee (2012) have developed a semi-analytical method whereby the interaction of
the buoyant-jet core and entrainment fields is used to predict the flow trajectory and
merging properties. For a long row of plumes, the external flow field would not be
expected to cause a deflection of the axes of plumes far from the end points, provided
that the symmetry is not broken. Significant symmetry breaking in this arrangement
does not seem to have been reported.

Here, a method is developed to model a long row of plumes, as follows. In § 2,
an argument is made for the identification of the plume–ambient boundary with the
velocity-potential contours of the entrainment flow field. In § 3, this entrainment flow
is modelled as that induced by a row of line sinks with spacing a. On an interval of

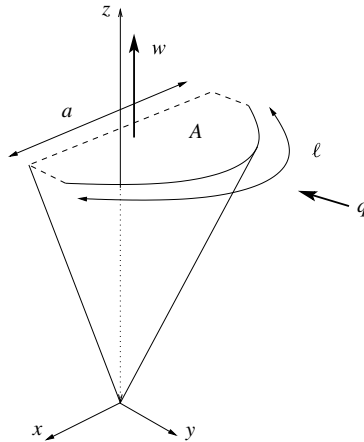† Email address for correspondence: gabriel.rooney@metoffice.gov.uk

FIGURE 1. A sketch of the half-plume flow under consideration, in a domain spanning $-a/2 \leqslant x \leqslant a/2$. A horizontal section of the half-plume has area A and top-hat vertical velocity w, and only entrains along a portion of the plume boundary, of length ℓ. Entrained fluid crosses the boundary with speed q.

length a with a line sink at its centre, the model is used to derive the area bounded by contours of velocity potential, and the flux across them. This interval forms the basis for modelling one plume (or jet) as the repeating unit in an infinite row, see figure 1. In §4, a model of a plume with arbitrary boundary shape is described, and the results derived previously are used to apply this to the repeating plume unit, and to develop an entrainment closure. The equations are solved numerically for the particular cases of rows of plumes and jets in an unstratified environment in §§5 and 6 respectively. Finally, an application of the model to flow in a channel is presented in §7.

2. The entrainment flow field and plume boundary

The complex potential of a line sink of strength $-m(z)$ at the origin is

$$\Omega = -\frac{m}{2\pi} \ln Z, \qquad (2.1)$$

where $Z = x + \mathrm{i}y$. This differs from the complex potential of a line vortex by only a factor of i. Kaye & Linden (2004) used a line sink to represent the converging, horizontal and irrotational flow exterior to a plume which is induced by plume entrainment (see also Taylor 1958).

The real part of the complex potential corresponds to the velocity potential. For a fluid of density ρ, Batchelor (1967, § 6.10) proposes a physical interpretation of the velocity potential as $(1/\rho)$ times the pressure impulse required to set up, or bring to rest, the irrotational velocity arising from the potential. In this sense, contours of equal velocity potential may be interpreted as connecting points at which an equal pressure impulse must be applied to bring about a given irrotational motion. Furthermore, the equations for mean plume motion are consistent with the assumption that the horizontal pressure gradient within the plume is neglected (Turner 1973, § 6.1.2), and thus the plume body is approximately isobaric at any given height.

Hence, contours of equal velocity potential may be used to approximate the mean plume boundary at different stages (i.e. heights) in the evolution of single or multiple

plumes. An additional feature of velocity-potential contours is that the flow is normal to the contours at all points, which would be expected of plume entrainment flow.

The total complex potential of an array of plumes, represented by line sinks, inherently incorporates the interaction of the flow fields induced exterior to the plumes.

3. Infinite row of line sinks

For an infinite array of parallel line sinks at positions na ($n \in \mathbb{Z}$), i.e. at intervals of length a along the real line, the total complex potential is

$$\Omega = -\frac{m}{2\pi} \ln \left(\sin \frac{\pi Z}{a} \right) + \Pi, \tag{3.1}$$

derived as in the vortex-street summation, e.g. Acheson (1990, § 5.7), where Π is an arbitrary constant. The velocity potential is

$$\begin{aligned}
\phi &= \operatorname{Re}(\Omega) \\
&= -\frac{m}{2\pi} \ln \left| \sin \frac{\pi Z}{a} \right| + \Pi \\
&= -\frac{m}{2\pi} \ln \left| \sin x' \cosh y' + \mathrm{i} \cos x' \sinh y' \right| + \Pi, \tag{3.2}
\end{aligned}$$

where $x' + \mathrm{i}y' = \pi Z/a$ and hence $x'/\pi = x/a$, etc. The velocity components u and v may be obtained from the complex derivative, $\mathrm{d}\Omega/\mathrm{d}Z = u - \mathrm{i}v$. In this case,

$$\frac{\mathrm{d}\Omega}{\mathrm{d}Z} = -\frac{m}{2a} \cot \frac{\pi Z}{a} = -\frac{m}{2a} \left(\frac{\sin 2x' - \mathrm{i} \sinh 2y'}{\cosh 2y' - \cos 2x'} \right). \tag{3.3}$$

The flow speed is given by $q = |\mathrm{d}\Omega/\mathrm{d}Z|$, hence

$$q^2 = \frac{m^2}{4a^2} \frac{\sin^2 2x' + \sinh^2 2y'}{(\cosh 2y' - \cos 2x')^2} = \frac{m^2}{4a^2} \frac{\cosh^2 2y' - \cos^2 2x'}{(\cosh 2y' - \cos 2x')^2}. \tag{3.4}$$

From (3.2), the contours of equal velocity potential are given by

$$\left| \sin \frac{\pi Z}{a} \right| = p, \tag{3.5}$$

where p is constant, or in terms of x' and y',

$$\cosh 2y' = 2p^2 + \cos 2x'. \tag{3.6}$$

Hence,

$$y' = \tfrac{1}{2} \ln(2p^2 + \cos 2x' + [(2p^2 + \cos 2x')^2 - 1]^{1/2}). \tag{3.7}$$

Figure 2 shows this solution plotted for a range of p. It is periodic in x' with period π, has roots at $x' = \pm(1/2) \cos^{-1}(1 - 2p^2)$ for $0 \leqslant p \leqslant 1$, and tends to a constant value of $\ln 2p$ as p tends to infinity. Its maximum value in the domain $-\pi/2 \leqslant x' \leqslant \pi/2$ is $y'_0 = (1/2) \ln(2p^2 + 1 + 2[p^2(p^2 + 1)]^{1/2})$ at $x' = 0$. The area under (3.7) is

$$A' = \int_{x'_-}^{x'_+} y' \,\mathrm{d}x', \tag{3.8}$$
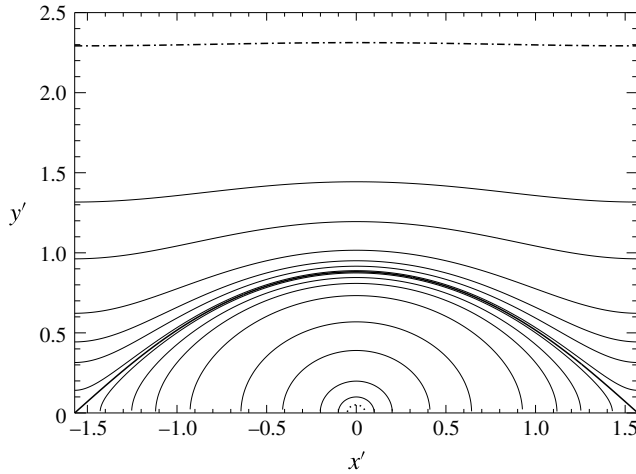
FIGURE 2. Contours of velocity potential. The corresponding values of p are those in table 1 in the range $0.05 \leqslant p \leqslant 5$. The domain spans $-\pi/2 \leqslant x' \leqslant \pi/2$. The contour $p = 0.05$ is dotted, and $p = 5$ is dot-dashed. The contour $p = 1$ is the thicker solid line which extends into the lower corners of the plot.

where

$$x'_\pm = \begin{cases} \pm(1/2)\cos^{-1}(1-2p^2), & 0 \leqslant p < 1, \\ \pm\pi/2, & p \geqslant 1; \end{cases} \tag{3.9}$$

A' is a function of p only, and is related to the actual area A by $A' = \pi^2 A/a^2$.

From (3.4) and (3.6), the flow speed at points along a particular velocity-potential contour satisfies

$$q^2 = \frac{m^2}{4a^2}\frac{p^2 + \cos 2x'}{p^2} = \frac{m^2}{4a^2}\frac{\cosh 2y' - p^2}{p^2}. \tag{3.10}$$

The flow is directed towards the origin.

The contour length is not used directly in the plume analysis; however, its calculation is a model for the calculation of the entrainment flux, which follows. It is also of interest to observe its evolution alongside the other derived quantities. First, (3.6) may be differentiated to obtain

$$\sinh^2 2y'\left(\frac{dy'}{dx'}\right)^2 = \sin^2 2x', \tag{3.11}$$

and hence

$$\left(\frac{dy'}{dx'}\right)^2 = \frac{\sin^2 2x'}{(2p^2 + \cos 2x')^2 - 1} = \frac{1 - (\cosh 2y' - 2p^2)^2}{\sinh^2 2y'}. \tag{3.12}$$

The length of the contour in the upper half-plane is

$$\ell' = \int_{x'_-}^{x'_+} d\ell', \tag{3.13}$$

where $d\ell'^2 = dx'^2 + dy'^2$. For $p > 1$, the length is given by

$$\ell' = \int_{x'_-}^{x'_+} \left(1 + \frac{\sin^2 2x'}{(2p^2 + \cos 2x')^2 - 1}\right)^{1/2} dx'. \tag{3.14}$$

For $p < 1$, numerical evaluation of ℓ' is complicated by the divergence of dy'/dx' at $x'_\pm$, and it is convenient to split the integral into pieces. Defining

$$x'_{\pm/2} = \tfrac{1}{2}x'_\pm = \pm\tfrac{1}{4}\cos^{-1}(1 - 2p^2) \tag{3.15}$$

and $y'_{+/2}$ as the value obtained by substituting for $x'_{+/2}$ into (3.7), then

$$\ell' = \int_{x'_{-/2}}^{x'_{+/2}} \left(1 + \frac{\sin^2 2x'}{(2p^2 + \cos 2x')^2 - 1}\right)^{1/2} dx'$$
$$+ 2\int_0^{y'_{+/2}} \left(1 + \frac{\sinh^2 2y'}{1 - (\cosh 2y' - 2p^2)^2}\right)^{1/2} dy'. \tag{3.16}$$

For $p = 1$, the length may be evaluated as

$$\ell' = \int_{x'_-}^{x'_+} \left(\frac{4 + 4\cos 2x'}{4 + 4\cos 2x' - \sin^2 2x'}\right)^{1/2} dx'. \tag{3.17}$$

Given the orthogonality of streamlines and velocity-potential contours, the flux E across the plume–ambient boundary in the upper half-plane is simply

$$E = \int_{x_-}^{x_+} q d\ell = \frac{mI}{2\pi}, \tag{3.18}$$

where

$$I = \int_{x'_-}^{x'_+} \frac{2aq}{m} d\ell'. \tag{3.19}$$

Like A', I is a function of p only. It may be evaluated in a similar manner to ℓ' using (3.10). Values of the main variables for a range of values of p are shown in table 1.

4. Generalised plume equations

To make use of the results from the previous section, it is convenient to write equations for flow in a half-plume. This will also simplify the later application. The half-plume (Boussinesq) equations may be written in a general form

$$A\frac{d}{dz}\left(\frac{1}{2}w^2\right) = Ag' - wE, \tag{4.1a}$$

$$\frac{d}{dz}(Aw) = E, \tag{4.1b}$$

$$\frac{d}{dz}(Awg') = -AwN^2, \tag{4.1c}$$

p	y_0'/π	x_+'/π	A'/π^2	ℓ'/π	I	I/ℓ'
0.05	0.01591	0.01592	0.00040	0.05863	3.68413	20.00259
0.10	0.03178	0.03188	0.00159	0.11727	3.68602	10.00512
0.20	0.06325	0.06409	0.00637	0.23468	3.69370	5.00986
0.40	0.12415	0.13099	0.02552	0.47115	3.72509	2.51669
0.60	0.18106	0.20483	0.05794	0.71473	3.78073	1.68378
0.80	0.23322	0.29517	0.10594	0.98210	3.87181	1.25489
0.90	0.25747	0.35643	0.13839	1.14295	3.94430	1.09848
0.95	0.26915	0.39892	0.15841	1.24452	3.99858	1.02271
0.99	0.27829	0.45495	0.17851	1.36584	4.07470	0.94961
1.00	0.28055	0.50000	0.18561	1.18013	3.14159	0.84736
1.01	0.28280	0.50000	0.19270	1.13215	3.14158	0.88327
1.05	0.29166	0.50000	0.21294	1.08721	3.14156	0.91978
1.10	0.30250	0.50000	0.23333	1.06255	3.14159	0.94113
1.20	0.32339	0.50000	0.26737	1.03812	3.14160	0.96328
1.50	0.38030	0.50000	0.34553	1.01341	3.14159	0.98677
2.00	0.45952	0.50000	0.44001	1.00401	3.14160	0.99601
5.00	0.73607	0.50000	0.73290	1.00010	3.14159	0.99990
10.00	0.95436	0.50000	0.95357	1.00001	3.14159	0.99999
15.00	1.08299	0.50000	1.08263	1.00000	3.14159	1.00000

TABLE 1. Values of the main variables described in § 3, for different values of p.

where w is the vertical velocity, g' is the reduced gravity and N^2 is the buoyancy frequency of the environment. The configuration is shown in figure 1. Equation (4.1a) is a combination of the usual volume-flux and momentum-flux equations. In this form it emphasises that the plume acceleration is a combination of buoyancy acting on the plume body and drag from entrainment acting on the plume boundary. The plume shape determines the relative strengths of these (Cenedese & Linden 2014).

Equations (4.1) revert to the (top-hat) axisymmetric (Morton, Taylor & Turner 1956) or two-dimensional (Lee & Emmons 1961; Stothers 1989) plume equations upon substituting the usual forms for the area and entrainment in those cases,

$$A = \tfrac{1}{2}\pi b^2, \quad E = \pi b \alpha w, \tag{4.2a,b}$$

$$A = ad, \quad E = a\alpha w, \tag{4.2c,d}$$

where α is an entrainment constant, b is the plume radius in the axisymmetric case (4.2a,b), d is the plume half-width in the two-dimensional case (4.2c,d) and a in this limit becomes an arbitrary length along the line plume (which cancels out).

From (3.10), the speed of entrained fluid at the centreline of the domain ($x' = 0$) is

$$q_0 = \frac{m}{2a} \frac{(p^2+1)^{1/2}}{p}. \tag{4.3}$$

One possible form of entrainment closure in the general case is to assume $q_0 = \alpha w$. This is the same as the conventional entrainment assumption in the limiting axisymmetric and two-dimensional cases, where the entrainment flow speed is uniform along the plume perimeter. The strength of the line sink is then determined from the plume velocity w and the value of p as

$$m = 2a\alpha w \frac{p}{(p^2+1)^{1/2}}. \tag{4.4}$$

Finally, it may be observed that, at any given height, if A and a are known, then the value of p may be determined by inverting (3.8), e.g. by root finding. That is, the 1:1 relationship between p and A' means that any function of p only can be represented equivalently as a function of A' only. Thus, m and I can be obtained from the values of A, a, α and w. The entrainment assumption is therefore sufficient to close the general equations (4.1).

5. Merging plumes in an unstratified environment

In an unstratified environment, (4.1*c*) may be integrated to obtain the conserved half-plume buoyancy flux, $B = Awg'$. Using (3.18) and (4.4), the remaining equations become

$$\frac{\mathrm{d}w}{\mathrm{d}z} = \frac{B}{Vw} - \frac{a\alpha}{\pi}\frac{w^2}{V}f, \tag{5.1a}$$

$$\frac{\mathrm{d}V}{\mathrm{d}z} = \frac{a\alpha}{\pi}wf, \tag{5.1b}$$

where $V = Aw$ is the half-plume volume flux and

$$f = \frac{p}{(p^2 + 1)^{1/2}}I \tag{5.2}$$

is a function of p only. Non-dimensionalising (5.1) using

$$w = \left(\frac{\alpha}{\pi}\right)^{-1/3}B^{1/3}a^{-1/3}\bar{w}, \quad V = \left(\frac{\alpha}{\pi}\right)^{-1/3}B^{1/3}a^{5/3}\bar{V}, \quad z = \left(\frac{\alpha}{\pi}\right)^{-1}a\bar{z} \tag{5.3a-c}$$

yields the equivalent equations in dimensionless variables, denoted by an overbar $^-$,

$$\frac{\mathrm{d}\bar{w}}{\mathrm{d}\bar{z}} = \frac{1}{\bar{V}\bar{w}} - \frac{\bar{w}^2}{\bar{V}}f, \tag{5.4a}$$

$$\frac{\mathrm{d}\bar{V}}{\mathrm{d}\bar{z}} = \bar{w}f. \tag{5.4b}$$

Requiring that $\bar{A} = \bar{V}/\bar{w}$ then implies $\bar{A} = A/a^2 = A'/\pi^2$.

For small values of p, the plume is expected to be approximately axisymmetric. In the axisymmetric case, the parameter describing the departure from the pure-plume similarity solution in the near-source region is

$$\Gamma(z) = \frac{5}{8\pi^{1/2}\alpha}\frac{(2B)(2V)^2}{(2M)^{5/2}} = \frac{5}{2^{5/2}\pi^{3/2}}\bar{A}^{-1/2}\bar{w}^{-3} \tag{5.5}$$

(Hunt & Kaye 2005; Devenish, Rooney & Thomson 2010), where $M = Vw$ is the half-plume momentum flux. Thus, $\Gamma = 1$ for a plume in which the fluxes are in balance with the similarity solution, while $\Gamma \to 1$ as $z \to \infty$ for plumes with arbitrary source conditions. Initial conditions for the integration of (5.4) can be generated by first choosing a small value of p (here 0.05) and hence the corresponding value of $\bar{A}$. Choosing a value of $\Gamma_0 = \Gamma(0)$ then sets the initial value of $\bar{w}$ using (5.5), and hence also $\bar{V}$. Solutions can then be compared for initial conditions of pure, forced or lazy plumes (respectively $\Gamma_0 = 1$, $\Gamma_0 = 0.1$, $\Gamma_0 = 10.0$).
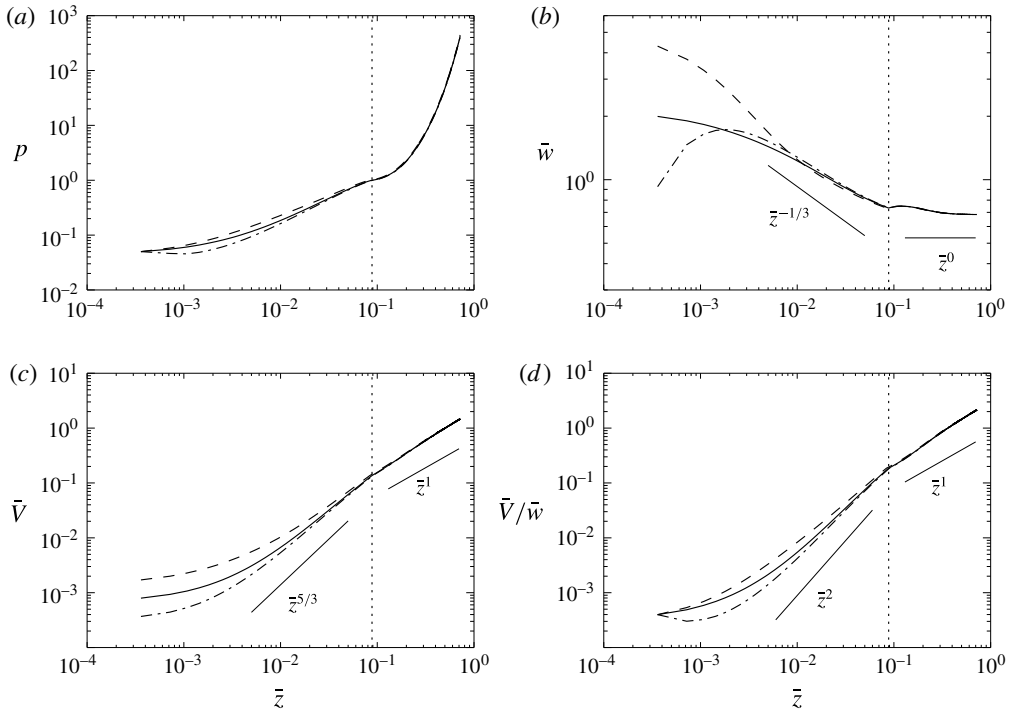
FIGURE 3. Results of integrating the unstratified plume equations (5.4). Pure ($\Gamma_0 = 1$), forced ($\Gamma_0 = 0.1$) and lazy ($\Gamma_0 = 10$) initial conditions are represented by solid, dashed and dot-dashed lines respectively. The solid straight lines show the similarity scalings for axisymmetric ($p < 1$) and line ($p > 1$) plumes. The dotted vertical lines mark $\bar{z} = 0.088$, where p is closest to 1 for the pure plume.

Equations (5.4) were integrated upward in the range $0.00036 \leqslant \bar{z} \leqslant 0.72$ using the fourth-order Runge–Kutta method with step size $\Delta \bar{z} = 0.00036$. The value of p is obtained from the half-plume area at each height step, for input to the next increment calculation.

Results are shown in figure 3. From the height at which the value of p is closest to unity, the pure, forced and lazy plumes begin to merge at $\bar{z} = 0.088$, 0.084 and 0.090 respectively. These results do not include an adjustment for the virtual source, which is discussed further in § 7.

Taking $\alpha = 0.1$ indicates that the pure-plume row begins to merge at $z/a \approx 2.76$. This is approximately 30 % lower than the height for full merging observed for two equal plumes by Kaye & Linden (2004). However, it appears to be comparable with, or perhaps higher than, the height at which merging was observed to begin for two plumes, from the example in figure 13 of Kaye & Linden (2004).

Figure 3 shows that the solutions approach the similarity predictions for axisymmetric plumes and line plumes below and above the merging height respectively. The lazy-plume solution shows that p may vary non-monotonically with $\bar{z}$, in this case because of flow contraction above the lazy-plume source. Fitting a line to the $\bar{V}$ data for $0.5 \leqslant \bar{z} \leqslant 0.72$ and extrapolating backward indicates that the line-plume virtual origin is above the source in all cases, with values of $\bar{z} = 0.038$, 0.033 and 0.040 for the pure, forced and lazy cases respectively.
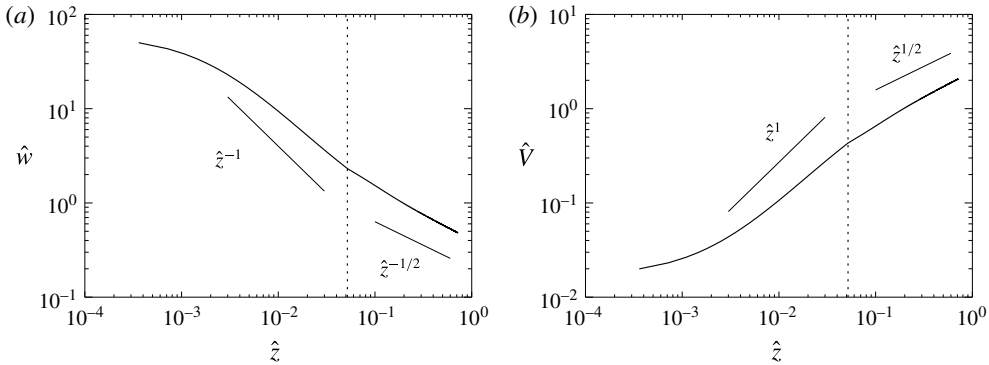
771 R1-8

FIGURE 4. Results of integrating the unstratified jet equation (6.2). The solid straight lines show the similarity scalings for axisymmetric ($p < 1$) and line ($p > 1$) jets. The dotted vertical lines mark $\hat{z} = 0.052$, where p is closest to 1 for the jet.

6. Merging jets in an unstratified environment

Where the source and the environment are both of the same density, then $B = 0$ and the equations represent the merging of jets. Equations (5.1) combine to show that M is now constant and (5.1b) becomes

$$\frac{dV}{dz} = \frac{a\alpha M}{\pi}\frac{f}{V} \tag{6.1}$$

or

$$\frac{d\hat{V}}{d\hat{z}} = \frac{f}{\hat{V}} \tag{6.2}$$

upon non-dimensionalising using

$$V = M^{1/2}a\hat{V}, \quad z = \left(\frac{\alpha}{\pi}\right)^{-1}a\hat{z}. \tag{6.3a,b}$$

If $w = M^{1/2}a^{-1}\hat{w}$ and $\hat{V}/\hat{w} = \hat{A} = A/a^2$, then conservation of M implies that $\hat{A}\hat{w}^2 = 1$, and hence a choice of $p = 0.05$ is sufficient to set the initial conditions in this case. It should be noted that $\hat{A} = \bar{A}$, and $\hat{z} = \bar{z}$ apart from differences in the value of α between the plume and jet cases.

The jet solution is shown in figure 4, and predicts a merging height of $\hat{z} = 0.052$. Fitting a line to the $\hat{V}^2$ data for $0.5 \leqslant \hat{z} \leqslant 0.72$ and extrapolating backward indicates that the line-jet virtual origin is also above the source, at $\hat{z} = 0.035$.

7. Plume rise in a channel

Bush & Woods (1998, figure 2) present experimental results on the depth of a two-dimensional outflow, resulting from plume rise from a source at the centre of the floor of a non-rotating channel. The experimental configuration is shown in figure 5. It is shown that as the channel becomes relatively narrower, the scaled depth of the outflow decreases. This is attributed to the reduction in plume entrainment associated with the influence of the channel walls on the plume flow.
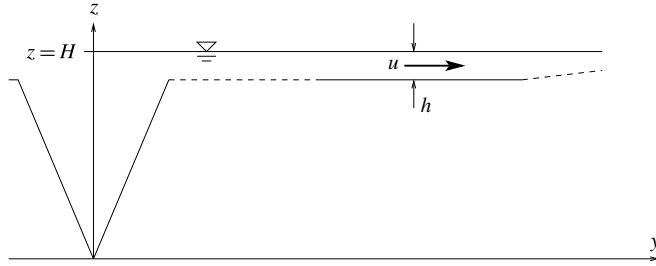
FIGURE 5. The experimental configuration of Bush & Woods (1998). The diagram shows a section along one half of the saltwater channel, of depth H and width (into the page) a. The position $y = 0$ marks the channel halfway point. The freshwater plume source is at the origin in the centre of the channel floor, and the plume produces currents flowing in both the positive and negative y directions. Measurements of current depth h were made at positions $y > H$, but always at distances greater than a from the end of the channel.

In the present notation, the predicted outflow depth scale for a wide channel is derived by Bush & Woods (1998) by assuming that continuity implies $V_H = uah$ and taking $u \sim (g'_H h)^{1/2}$, where V_H is the half-plume volume flux at the top of the channel of height H, a is the channel width, and u, g'_H and h are the outflow speed, reduced gravity and depth respectively. Combining these with the axisymmetric-plume similarity solution prediction of $V_H \sim B^{1/3} H^{5/3}$ and $g'_H \sim B^{2/3} H^{-5/3}$ yields the wide-channel depth prediction of

$$\frac{h}{H} = C_1 \left(\frac{H}{a} \right)^{2/3}, \tag{7.1}$$

where C_1 is a dimensionless constant determined experimentally. As the channel narrows, the plume flow departs from the similarity solution and entrains less. The experimental data show the depth to take the general form

$$\frac{h a^{2/3}}{H^{5/3}} = r, \tag{7.2}$$

where r is an unknown decreasing function of the aspect ratio H/a.

The model of the previous sections may be applied to this case, since the 'plume in an infinite row of plumes' is also a representation of plume rise in a channel using the method of images. This again assumes an absence of symmetry breaking by small perturbations, and neglects any boundary-layer effects from the channel walls which may act as a drag on the entrainment flow at the edges.

Thus, the equivalent model here takes $V_H = uah$ and $u \sim (g'_H h)^{1/2}$ as above, and substitutes $g'_H = B/V_H$ to obtain $(h/a) \propto V_H/(B^{1/3} a^{5/3})$ or

$$\frac{h a^{2/3}}{H^{5/3}} = C_2 \left(\frac{\alpha}{\pi} \right)^{4/3} \frac{\bar{V}_H}{\bar{H}^{5/3}}, \tag{7.3}$$

where, following (5.3c),

$$\bar{H} = \left(\frac{\alpha}{\pi} \right) \frac{H}{a} \tag{7.4}$$
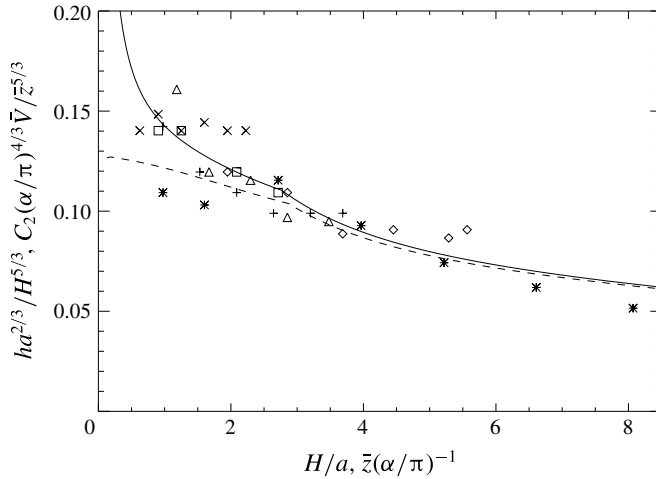
FIGURE 6. Comparison of the model output with the data of Bush & Woods (1998). The solid line shows the pure-plume model with a proportionality constant of $C_2 = 1.4$. The dashed line shows the same model with an optimal virtual-origin correction incorporated. The symbols $*$, $\diamond$, $+$, $\triangle$, $\square$ and $\times$ correspond to scaled outflow-depth measurements in channels of width 4, 6, 9, 10, 12 and 15 cm respectively. Bush & Woods (1998) indicate an experimental error of approximately ± 0.013 in the scaled depths.

and C_2 is a dimensionless constant to be determined. Hence, plotting $ha^{2/3}/H^{5/3}$ against H/a for the data of Bush & Woods (1998) is equivalent to plotting $C_2(\alpha/\pi)^{4/3}\bar{V}/\bar{z}^{5/3}$ against $\bar{z}(\alpha/\pi)^{-1}$ from the (pure) plume integration. The comparison is shown in figure 6, where a typical value of $\alpha = 0.1$ has been assumed. It may be seen that taking $C_2 = 1.4$ produces a satisfactory fit to the data (solid line).

Figure 6 also shows that the current-depth equivalent from the model data diverges at very small values of z/a rather than tending to the wide-channel limit. This divergence may be attributed to the departure of the pure-plume numerical solution from the similarity scaling at small values of $\bar{z}$, which is mainly due to the lack of virtual-origin correction. The numerical model has an initial 'radius' b_0 given by $b_0/a \approx 0.0159$ (see table 1) at the first model level $\bar{z}_1 = 0.00036$. From the axisymmetric pure-plume similarity solution $b = 6\alpha z/5$ (Morton *et al.* 1956), the depth of the virtual origin $\bar{z}_v$ would be given by

$$\bar{z}_v + \bar{z}_1 = \frac{5}{6\pi}\frac{b_0}{a}, \qquad (7.5)$$

hence $\bar{z}_v \approx 0.0039$. The optimal value for convergence at small $\bar{z}$ is found to be $\bar{z}_v \approx 0.0034$, approximately 87 % of the theoretical axisymmetric-plume value (and 4 % of the pure-plume merging height). The model data with this correction (i.e. $\bar{z}$ replaced by $\bar{z} + \bar{z}_v$) are plotted as the dashed line in figure 6. The model now tends to a wide-channel value of approximately 0.13, which is also the best estimate of C_1 by Bush & Woods (1998). Virtual-origin correction is not discussed by Bush & Woods (1998), so it is possible that similar issues are responsible for some of the spread in the experimental data at low values of H/a.

8. Conclusion

A model has been presented whereby the physical interpretation of the velocity potential of plume entrainment flow is used to define contours of the plume–ambient boundary. This has been applied to the case of an infinite row of plumes, represented by line sinks, in which the velocity potential is of a known form. The plume equations have been written in a generalised form for a boundary of arbitrary shape, and it has been shown that an entrainment assumption is sufficient to close the resulting equations.

Integration of the model shows it to approach the limiting forms of axisymmetric and two-dimensional plume or jet flow below and above the merging height. The derived merging heights are found to be lower than those observed in the merging of two equal plumes. The model also predicts the virtual-source position of the far-field flows. An application of the model to the case of plume rise in a channel shows that it can be used to predict the depth of the resulting horizontal outflow satisfactorily, for a range of channel widths and aspect ratios.

The model has been solved here using an assumption of constant α. It would also be possible to use a more sophisticated entrainment assumption relating α to the curvature of the plume–ambient boundary. This may be appropriate if the turbulence structure, and hence entrainment strength, can similarly be related.

Acknowledgements

References

ACHESON, D. J. 1990 *Elementary Fluid Dynamics*. Oxford University Press.

BATCHELOR, G. K. 1967 *An Introduction to Fluid Dynamics*. Cambridge University Press.

BUSH, J. W. M. & WOODS, A. W. 1998 Experiments on buoyant plumes in a rotating channel. *Geophys. Astrophys. Fluid Dyn.* **89** (1–2), 1–22.

CENEDESE, C. & LINDEN, P. F. 2014 Entrainment in two coalescing axisymmetric turbulent plumes. *J. Fluid Mech.* **752**, R2.

DEVENISH, B. J., ROONEY, G. G. & THOMSON, D. J. 2010 Large-eddy simulation of a buoyant plume in uniform and stably stratified environments. *J. Fluid Mech.* **652**, 75–103.

HUNT, G. R. & KAYE, N. B. 2005 Lazy plumes. *J. Fluid Mech.* **533**, 329–338.

KAYE, N. B. & LINDEN, P. F. 2004 Coalescing axisymmetric turbulent plumes. *J. Fluid Mech.* **502**, 41–63.

LAI, A. C. H. & LEE, J. H. W. 2012 Dynamic interaction of multiple buoyant jets. *J. Fluid Mech.* **708**, 539–575.

LEE, S.-L. & EMMONS, H. W. 1961 A study of natural convection above a line fire. *J. Fluid Mech.* **11**, 353–368.

MORTON, B. R., TAYLOR, G. I. & TURNER, J. S. 1956 Turbulent gravitational convection from maintained and instantaneous sources. *Proc. R. Soc. Lond.* A **234**, 1–23.

STOTHERS, R. B. 1989 Turbulent atmospheric plumes above line sources with an application to volcanic fissure eruptions on the terrestrial planets. *J. Atmos. Sci.* **46**, 2662–2670.

TAYLOR, G. I. 1958 Flow induced by jets. *J. Aero. Sci.* **25**, 464–465.

TURNER, J. S. 1973 *Buoyancy Effects in Fluids*. Cambridge University Press.